**Taking Nanotechnological Remediation Processes
from Lab Scale to End User Applications
for the Restoration of a Clean Environment**

Project Nr.: 309517
EU, 7th FP, NMP.2012.1.2

**WP2: Design, Improvement and Optimized Production of
Nanoparticles – Zero-Valent Iron Nanoparticles – nZVI**

**DL 2.2: Assessment of Nanoparticle Performance
for the Removal of Contaminants – nZVI Particles**

Miroslav Černík, Kristýna Pešková (TuLib), Jan Filip (UPOL),
Vi-cens Marti (CTM), Melanie Auffan (CNRS-CEREGE)

30 September 2016

List of co-authors:

Name, First Name	Partner Organisation	
Cernik, Miroslav Peskova, Kristyna Nosek, Jaroslav Petr Parma	Technical University of Liberec	
Slunsky, Jan	Nano Iron, s.r.o.	
Kamptner, Andre	UVR-FIA Verfahrensentwicklung - Um-weltschutztechnik - Recycling GmbH	
Filip, Jan Zboril, Radek	Palacky University Olomouc	
Marti, Vicens Benito, Josep Ribas, David	Fundacio CTM Centre Technologic	
Auffan, Melanie	Centre National de la Recherche Sci-etifique	

Reviewed by PAG member(s):

Name, First Name	Organisation	
Matz, Pierre	Solvay Brussels, Belgium	
Elliott, Daniel	Geosyntec Consultants, USA	
Bruns, Johannes	Intrapore, Germany	

Reviewed and agreed by PMG

Table of Contents

List of Figures

List of Tables

Glossary

BET	Brunauer-Emmet_Teller theory (estimation of specific surface area)
CEs	Chlorinated Ethenes
CIP	Carbonyl Iron Powder
CHCs	Chlorinated Hydrocarbons
CMC	Carboxy Methyl Cellulose
d_p	Particle Diameter
EDX	Energy-Dispersive X-ray Spectroscopy
GC/MS	Gas Chromatography – Mass spectroscopy
GW	Groundwater
HAADF	High Angle Annuar Dark Field
ICP-AES	Inductively Coupled Plasma - Atomic Emission Spectrometry
MEG	MonoEthylenGlycol
NPs	Nanoparticles
nZVI	Nano-scale ZeroValent Iron
PCE	Perchlorethylene
SEM	Scanning Electron Microscopy
TCE	Trichloroethene
TEM	Transmission Electron Microscopy
WP	Work Package
XANES	X-ray Absorption Near Edge Spectroscopy
XRD	X-ray Diffraction
XRF	X-ray Fluoresence Spectroscopy

1   Introduction

1.1   Background

NanoRem ("Taking Nanotechnological Remediation Processes from Lab Scale to End User Applications for the Restoration of a Clean Environment") is a research project, funded through the European Commission's Seventh Framework Programme.

The overarching aim of NanoRem is to support and develop the appropriate use of nanotechnology for contaminated land and brownfield remediation and management in Europe. NanoRem focuses on facilitating the practical, economic and exploitable nanotechnology for in-situ remediation. This can only be achieved in parallel with a comprehensive understanding of: the environmental risk-benefit balance for the use of nanoparticles (NPs).

1.2   Introduction to DL2.2 and DL3.2

Work packages WP2 and WP3 of NanoRem deal with the design, improvement and optimized production of nanoparticles for *in-situ* remediation. WP2 is focused on Zero-Valent Iron Nanoparticles – nZVI and WP3 on Non-ZVI and Composite Particles. The final deliverables DL2.2 (Assessment of Nanoparticle Performance for Removal of Contaminants – nZVI Particles) and DL3.2 (Assessment of Nanoparticle Performance for Removal of Contaminants – Non-ZVI and Composite Particles) of the two WPs give an overview of the application areas and potential of the nanoparticles developed and aim to provide decision-making tools for problem owners and authorities. The two reports follow the same structure and should be seen as complementary. Table 1 provides an overview on the nanoparticle types presented in each of the two report deliverables. DL3.2 and DL3.3 mainly focus on the physical and chemical properties and reactivity of the nanoparticles. Particle transport, delivery and suspension stability are covered in DL4.2 (Stability, Mobility, Delivery and Fate of optimized NPs under Field Relevant Conditions).

Table 1:   Overview of the nanoparticle types presented in DL2.2 and DL3.2

DL2.2	DL3.2
NANOFER 25P	Nanoiron-oxide (Nano-Goethite)
NANOFER 25S	Carbo-Iron®
NANOFER STAR	Trap-Ox Fe-zeolites
FerMEG12 (A02, KKM02, nZVI-Labstar, KKM13)	(Palladized) Bionanomagnetite
Abrasive milling nZVI (NA56, NA64, NA74, NA84)	Non-ZVI metals (Mg/Al particles, Nano-FerAl)
	Barium Ferrate

2 Objectives of DL 2.2

The objectives of DL 2.2 are to provide an overview of the ZVI nanoparticles produced and studied during the project and their main characterization, physical and chemical properties and their application areas based on the performed laboratory experiments.

Various types of nZVI materials are available on the market, supplied mainly in the form of an aqueous suspension. NZVI is gradually oxidized due to its reaction with water, where the content of the active phase (Fe(0)) is significantly reduced in the product. Increased transport costs (due to the presence of water in the product) together with massive aggregation of nanoparticles, which tends to lead to poor migration properties and low reactivity are major problems that make the whole application significantly more expensive and less successful. Moreover the uncertain time delay between production and use, for the nZVI aqueous suspensions, is also an important factor from this point of view. The longer the time delay the less reactive the material.

The development of an air-stable nZVI production technology with the possibility to control the thickness of the oxide shell has led to the possibility of transporting the nZVI product in the form of a chemically stable powder without any significant loss of the active phase.

Air-stable nZVI can be stabilized secondarily by a suitable environmentally friendly organic surfactant to reduce the degree of aggregation of material and help to maximize the migration properties in the aquifer, which is also an important focus of this research. The secondary surface modification, which sits on top of the stabilizing oxide shell, can be done directly at the site, just before the application, thereby ensuring perfect migration properties and high quality of injected nZVI (i.e. cumulative effects of the oxide and organic layers do not significantly reduce nZVI reactivity).

The second research direction is focused on the preparation of nZVI by a less expensive technology, which is milling/grinding from larger ZVI particles (microscale Fe). The application potential of such a technology is extraordinary because it simultaneously reduces the cost of the application due to the lower cost of the precursor and the preparation technique (no hydrogen needs). Such a technology can be economically competitive with air-stable nZVI even with worse nZVI properties for the treatment of the contaminant.

The WP2 team members worked during the first period of the project on setting up large scale particle production and all of the supporting developments. The whole procedure can be mapped as follows: development of optimal particles for reactivity with chlorinated hydrocarbons and mobility in the aquifer on a laboratory scale, setting up large scale production based on these results, testing of production, nZVI characterization and comparison of nZVI produced in laboratory with the large scale production.

3   Overview of WP2 Nanoparticles

Three groups of nZVI-particles were produced within the WP2. The different production process for each group is described in brief below.

- nZVI produced by solid-thermal reduction of iron oxide powder

- milled iron nanoparticles

- milled iron nanoparticles with an abrasive (alumina)

3.1 ZVI nanoparticles produced by solid-thermal reduction of iron oxide powder

Pure nZVI powder without surface treatment (pyrophoric Fe, NANOFER 25P) was taken as a basis for production of the different nZVI nanoparticles used within the project. The 20% aqueous slurry (NANOFER 25), slurried surface modified nanoparticles (NANOFER 25S) and air-stable nZVI powder (NANOFER STAR) are the nanoparticles used and studied during the project. In the case of NANOFER STAR, the iron oxide shell stabilizes the surface of the nanoparticles and prevents their rapid oxidation ("burning" or fast water oxidation). A combination of various parameters during synthesis (an appropriate mixture of N_2, Ar and O_2 gases, temperature and time) affects the resulting thickness of the iron oxide shell and thus the properties of the resulting product. The proportion of the magnetite (Fe_3O_4)/maghemite (γ-Fe_2O_3) phase increases during the passivation process of the nZVI surface. The passivating oxide shell on the surface of the nanoparticles has been studied using transmission electron microscopy – the layer thickness varies from ~4 nm to ~20 nm depending on the passivation conditions. The shell thickness influences the stability, reactivity, storage and also the agglomeration of the nanoparticles. A layer of 4 nm seems to be adequate from more points of interest and preferred for the final product.

The production of nZVI with a combined shell is carried out in two steps: Firstly, the dry air-stable powder (NANOFER STAR) is produced by solid-state thermal reduction of iron oxide powder with final stabilization by addition of oxygen. Secondly, a selected organic surface modifier is incorporated into the solution (e.g. CMC) and the solution is dispersed in order to obtain a homogeneous suspension and break up agglomerated nanoparticles. The second step can be performed days or a week later and also on site. The produced suspension is then diluted to the final nZVI concentration.

At first, the production procedure was transferred to a semi-industrial scale and then to a full industrial scale by the company NANO IRON s.r.o. The NPs were tested in the laboratory and also in the field and are ready for market.

3.2 Milled iron nanoparticles

Milled ZVI NPs are produced in a two-stage top-down process. The basic raw material ATOMET 57, a coarse, high purity granulated iron powder from Rio Tinto, Quebec Metal Powders Ltd., is in the first stage grinded dry with inhibitors as corrosion protection up to a particles size of < 40 μm. The second stage uses wet grinding with mono ethylene glycol (MEG) as the grinding liquid and the addition of a surfactant. MEG was chosen to prevent NP oxidation during the milling process (compared to water) and to eliminate production of flaky-shaped nanostructures (milling in ethanol). Moreover, MEG is

water dilutable and biodegradable (i.e.: Ramakrishna et al., 2005), it is a common approach to use biodegradable dispersants which can enhance the overall remediation (Wei et al., 2012). Sieving is performed using a Dreßler type sieve in a dry process prior the fine wet grinding. Nano-structured, flake-shaped particles with thicknesses of less than 100 nm are the final product, called FerMEG12.

The production procedure at UVR-FIA GmbH was transferred to a large-scale production at an industrial level. The milled NPs were tested in the laboratory and in the field, and are ready for the market.

3.3   Milled iron nanoparticles with alumina as an abrasive

The addition of alumina has a positive effect on particle milling by breaking down the iron flakes obtained in the first milling step and also by producing nano iron particles from the abrasion of the grinding media. The initial iron powder was Carbonyl Iron Powder (CIP-SM, BASF). The millings were performed in a planetary ball mill (P-5, Fritsch) using hermetic steel vials with a capacity of 250 ml. The tests were divided in two 24h steps. Firstly, the flattened iron particles or flakes were produced and secondly, these flakes were broken down and smaller iron particles were obtained.

Almost 100% of the fraction of particles is under 1μm. This result was possible using a grinding media of 0.5 mm in diameter (iron balls) and an alumina concentration of 8.04g in 100ml.

The NPs were tested in the laboratory and their physical and chemical properties and reactivity were compared with commercially available NPs. The large scale production of the NPs is expected but it is not part of the project. It could be scaled up being a promising new economic method with high throughput and superior nZVI performance. CTM gave all the details of the process, a scale up experimental design and sample characterization work flow to UVR-FIA GmbH under an agreement on exploitation. CTM would like to explore the scale up feasibility and they are looking for other calls, partners or financial support to build a pilot ball mill.

4   Methods for Particle Characterization and Reactivity Studies

4.1   Particle characterisation techniques

Subsequently, the selected materials were characterized in detail to confirm the properties of the nZVI particles prior to disseminating them to NanoRem partners, with detailed measurements of the thickness of the developed oxide shell on the nZVI particles. A simple oxide shell allows nZVI a long-term storage on air, safe delivery and simple manipulation. On the other hand the protection is so good, that simple dilution in water cannot deactivate the protective layer and NP must be activated prior its application. The activation process involves preparing concentrated nZVI/water slurry (20% wt.) and keeps it for 48 hours. Different methods were employed for the nZVI characterization, including X-ray powder diffraction (XRD), [57]Fe Mossbauer spectroscopy, BET surface area measurements and scanning/transmission electron microscopy (SEM/TEM) combined with high angle annular dark field (HAADF). The experimental batches were prepared to check whether the changes in the preparation procedure parameters also have an effect on the nZVI properties during large-scale production. In addition to the content of Fe(0) analysed using the hydrogen production method, the total iron concentration was analysed by Inductively Coupled Plasma Atomic Emission Spectroscopy (ICP-AES). The ζ-Potentials were determined using electrophoretic light scattering (ZetaSizer Nano ZS).

X-ray powder diffraction (XRD)

X-Ray powder diffraction (XRD) was performed on a PANalytical X'Pert PRO MPD q/q Bragg-Brentano powder diffractometer using Cu-Kα radiation. Continuous scans from 12 to 120° 2θ were collected with a step size of 0.017° and a scan speed of $3.4 \cdot 10\text{-}3$ °·min^{-1}.

[57]Fe Mossbauer spectroscopy

Transmission [57]Fe Mössbauer spectra were collected at a constant acceleration mode with a [57]Co (Rh) source at room temperature. The isomer shift values were related to metallic a-Fe foil at 300 K.

BET surface area measurements

Nitrogen Brunauer-Emmett-Teller Specific Surface Area (SSA) was measured (ASAP 2020, Micromeritics, USA), degassing was carried out for several hours at a maximum temperature of 100ºC.

Scanning/transmission electron microscopy (SEM/TEM) combined with high angle annular dark field (HAADF)

For electron microscopy characterization, samples were prepared in a glove box under a nitrogen atmosphere with air locks (Jacomex 2P). The samples were suspended by mixing vigorously in absolute ethanol. For the SEM studies (Gemini ultra plus, Zeiss) the samples were deposited and left to evaporate on standard SEM discs. For the TEM studies (Philips CM30, operating at 300 kV) a droplet was placed on a 300 copper mesh grid with a supporting film made of holey carbon (S147-3, Agar Scientific). Pyrophoric samples were transferred to the microscope using a liquid nitrogen flask to avoid any contact with oxygen. Detailed nZVI surface observations were performed using a high-resolution transmission electron microscopy image (HRTEM) FEI Titan 60-300 microscope with an X-FEG type emission gun, operating at 80 kV.

Content of Fe(0) analysed using the hydrogen production method

The content of Fe(0) was analysed by triplicate through the hydrogen production method (Liu et al., 2005a) where the iron reacts with sulfuric acid added to the slurry and the volume of produced hydrogen is measured using an specific hardware (nZVI Tester, Nanoiron, Czech Republic).

Total iron concentration analysed by Inductively Coupled Plasma Atomic Emission Spectroscopy (ICP-AES)

Total iron concentration was assessed, firstly, digesting the suspensions with 2:1 $HNO_3:H_2O_2$ and then analysing it by Inductively Coupled Plasma Atomic Emission Spectroscopy (ICP-AES), (Optima 3200, Perkin-Elmer, USA).

The ζ-Potentials determined using electrophoretic light scattering (ZetaSizer Nano ZS)

ζ-potential was measured using dynamic light scattering and electrophoretic light scattering (Z-Sizer nano ZS, Malvern). The experiment started with the preparation of 1.0 g·l^{-1} suspensions of the nZVI and iron oxides with water at 0.01M (NaCl) ionic stretch. All procedure was done under nitrogen atmosphere that also served as agitation.

4.2 Reactivity studies

4.2.1 Batch experiments

Batch tests with a model contaminant (hexavalent chromium) were designed to determine the reactivity of the nZVI samples in activated and unactivated states. The reactivity tests with Cr(VI) (initial concentration of 50 mg/L) were performed in 100 hermetically closed bottles with different amounts of nZVI to obtain a final concentration of 0.1, 0.25, 0.5, 2.0, 2.5, 4.0 and 8.0 g/L. The solution was left to react for 24 hours with a bottom-up rotation every 60 s to avoid particle settling. The sampling interval was 2 and 24 hours. The decrease in the concentration of Cr(VI) and changes in the pH and ORP were monitored using a spectrophotometer (DR3900) and a multimeter (WTW 343i), respectively. The 24 h reaction time was chosen even though the preliminary batch tests showed that Cr(VI) depletion mainly took place within the first 2h.

The reactivity tests with chlorinated hydrocarbons (CHCs) were carried out with contaminated groundwater from WP10 field sites. The tests were carried out in 250 mL glass reagent bottles with a Teflon septum. To prevent volatilization, the sample containers were prepared separately for each measured time. The sample was placed in a vertical revolving shaker and subsequently analysed at specific times for CHC content by GC/MS (Varian 3800/Saturn 2800) and in each sample were monitored pH and ORP (WTW 343i). The natural rate of volatilization of the sample was evaluated based on an analysis of the control samples without nZVI.

4.2.2 Column experiments

For the column tests, a 2 m long column with an inner diameter of 2.5 cm was used. The column was oriented vertically such that influent groundwater flow was directed up and through the column, against gravity. The column was filled with monomineral sand with a grain size smaller than 1 mm. A funnel was used to fill the column as homogeneously as possible and the sand was compacted by

vibrating. In order to reduce the oxidation processes the column was flushed with nitrogen and saturated with degassed water. Groundwater was pumped through the column by two peristaltic pumps: a circulation pump (PCD825, Čerpadla Kouřil) providing the main water flow in the system (the water also passes through a MAD-02 degasser, REGOM INSTRUMENTS s.r.o.) and a dosing pump (PCD21, Čerpadla Kouřil) for continuous dosing of the aqueous nZVI suspension from a stirred tank, which was purged with argon to suppress the oxidation of nZVI. The concentration of iron in the column was monitored through measurement of magnetic susceptibility, which is significantly higher for zero-valent iron than for cationic forms. A scanner was specially designed for this measurement. The pressure was also monitored on the input of the column.

5 Application Areas and Potential Based on Reactivity and Physical-chemical Properties

5.1 nZVI particles NANOFER 25P, NANOFER 25S, NANOFER STAR

Responsible partner: NANOIRON, s.r.o.

The particles prepared by thermal reduction were tested and compared to each other and to other types of particles. The prepared particles were: NANOFER 25P (bare nZVI without any additional surface modification, pyrophoric iron), NANOFER 25S (nZVI with Polyacrylic acid (PAA) modification) and NANOFER STAR (nZVI with a thin oxide shell, air-stable).

Special attention was paid to the activation process of dry nZVI particles (NANOFER STAR). The NANOFER STAR particles exhibit relatively low reactivity with contaminants at low iron concentrations in water (only a few g/L) due, in part, to the presence of the oxide shell. The standard activation protocol is based on preparation of a 20% aqueous slurry which remains for up to 48 hours at room temperature without shaking or other treatment. After the activation process, which essentially involves the dissolution of the oxide layer, the slurry can be diluted to a final concentration for the experiment. The NPs with various oxide shells were compared with NANOFER STAR (batch 197) as a standard. Reactivity tests with artificially prepared contaminated samples and groundwater samples from contaminated sites were carried out with non-activated and activated particles. It was shown that the activation process is necessary for sufficient reactivity of NANOFER STAR. During the activation process, the surface of the NANOFER STAR particles dissolves and makes Fe(0) available for reduction reactions.

Additional NANOFER STAR surface modifications with various concentrations of carboxy methyl cellulose (CMC) were tested after the activation process.

5.1.1 Physical and chemical properties of NANOFER nZVIs

In order to study the thickness of the iron oxide layer, TEM images of particle shells were taken for all of the representative particles. The surface of the NANOFER 25P was not treated to be air stable; however, it presented a thin oxide layer with a mean thickness of 1.8 nm despite its pyrophoricity (Table 2 and Figure 1a). NANOFER STAR, batch 197 had a medium oxide layer compared to the other tested particles averaging 3.4 nm (Table 2and Figure 1b), which protecting it from pyrophoricity. NANOFER STAR, batch 400 showed the largest oxide layer with a mean thickness of 6.5 nm (Table 2 and Figure 1c A relatively stable thickness over the particles of the same class was

observed if measurements were taken where no overlays into aggregates boundaries were present (Figure 1).

After activation, NANOFER 25P and NANOFER STAR 197 showed a partial breakdown of the oxide shell and in general a decrease in thickness (Figure 1d, e, respectively). For NANOFER STAR 400 (Figure 1f), the breakdown of the oxide shell was observed less often, but there was a clear diminution in its thickness. Moreover, there was a clear negative relationship between oxide shell thickness and relative zero valent iron content, Table 2 and Table 3.

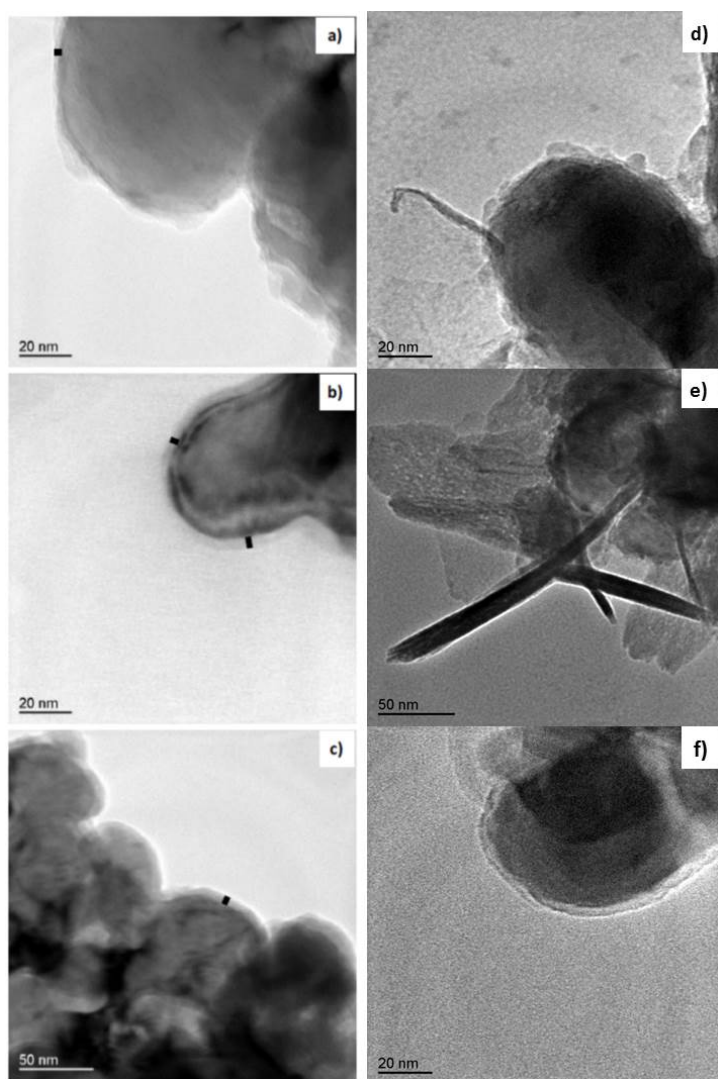**Figure 1:**   TEM images of particles. Not activated: a) NANOFER 25P, b) NANOFER STAR 197 and c) NANOFER STAR 400. Activated: d) NANOFER 25P, e) NANOFER STAR 197 and f) NANOFER STAR 400. The black bars show some of the measured zones

Table 2:   Mean thickness of the oxide layer in nm, 95% interval of confidence.

NANOFER 25P	NANOFER STAR 197	NANOFER STAR 400
1.8 ±0.98	3.4 ±1.49	6.5 ± 1.16

Table 3:   Relative Fe content in the selected iron nanoparticles. Results in weight percentages.

NANOFER 25P	NANOFER STAR 197	NANOFER STAR 400
84.3	72.9	56.2

An X-ray diffraction study was also performed to establish the composition of the oxide shell before and after activation. Sample preparation consisted in manual pressing the powder material in standard rectangular sample holders of 20 mm L x 15 mm W x 1 mm H (PW1172/01). The instrument was a PANalytical X'Pert PRO MPD q/q Bragg-Brentano powder diffractometer with a 240 mm radius using Cu Kα radiation (l = 1.5418 Å).

Figure 2 shows the XRD pattern for the non-activated (NANOFER STAR 400 NA) and activated (NANOFER STAR 400 A) NANOFER STAR, batch 400. In this material, the peaks corresponding to Fe(0) have a great intensity, which means clear crystallinity. This material had the lowest iron content, and correspondingly the peaks from the oxides are clearly visible. The vast majority of the peaks corresponded to magnetite (Fe_3O_4). The peaks were very close to those belonging to maghemite (γ-Fe_2O_3), but two positions associated to maghemite had no signals. Moreover, some small peaks were associated to Wuestite (FeO).

The differences between both diffraction patterns were very small, the peaks were the same and their relative intensities were very similar, which means that very small changes in crystalline Fe(0) and oxides were produced by the activation process.
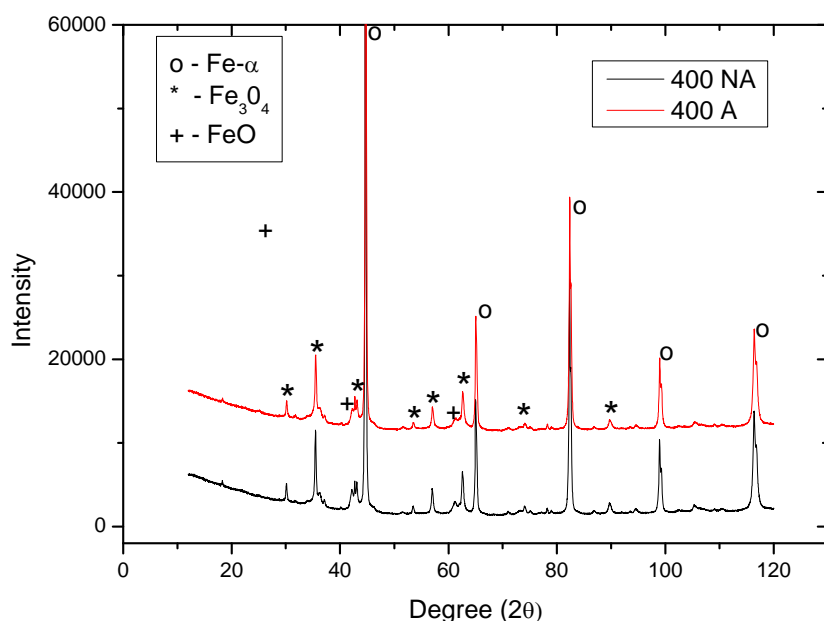
Figure 2:   XRD pattern for NANOFER STAR 400 in both states

Figure 3 shows the XRD patterns for the NANOFER STAR, batch 197 in both states and for NANOFER 25P after activation. For these samples, the Fe(0) content was less and the peaks belonging to magnetite and wuestite had less intensity and are sometimes difficult to recognize. Again, no important changes between activated and non-activated samples were observed.
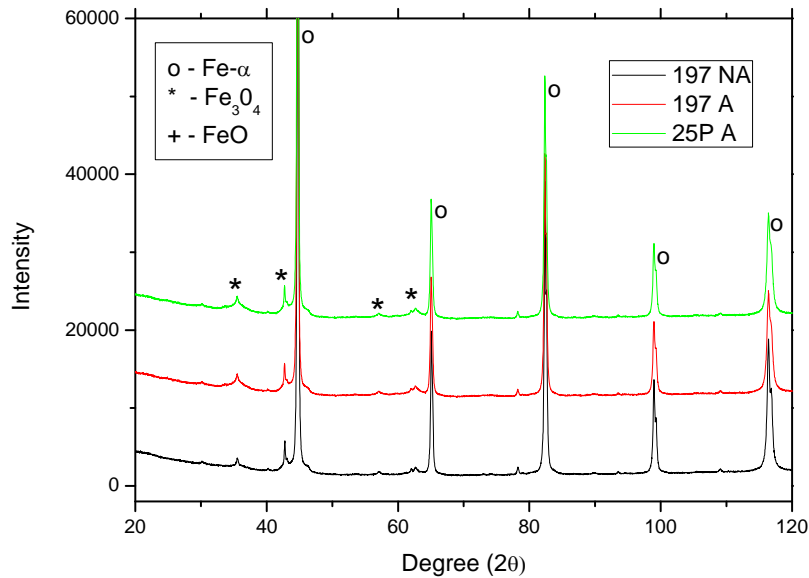
Figure 3:   XRD pattern for NANOFER STAR 197 activated (A) and non-activated (NA) and NANOFER 25P (A).

After refinement by the Rietveld method (the common data treatment to obtain semi quantitative compositions through XRD), a semi-quantitative analysis was performed using the peaks of the three species found, as shown in Figure 4. As it is shown in Table 4 for NANOFER STAR, batch 400 no differences were observed between the activated and non-activated states, and the total Fe(0) content determined by XRD was similar to that obtained by the H2 method. For the rest of the samples, in which the amount of crystalline oxides was clearly lower, it was difficult to perform a reliable quantification. In any case, the presence of Wuestite (FeO) in the oxide shell of NANOFER STAR, batch 197 and NANOFER 25P must be very weak.
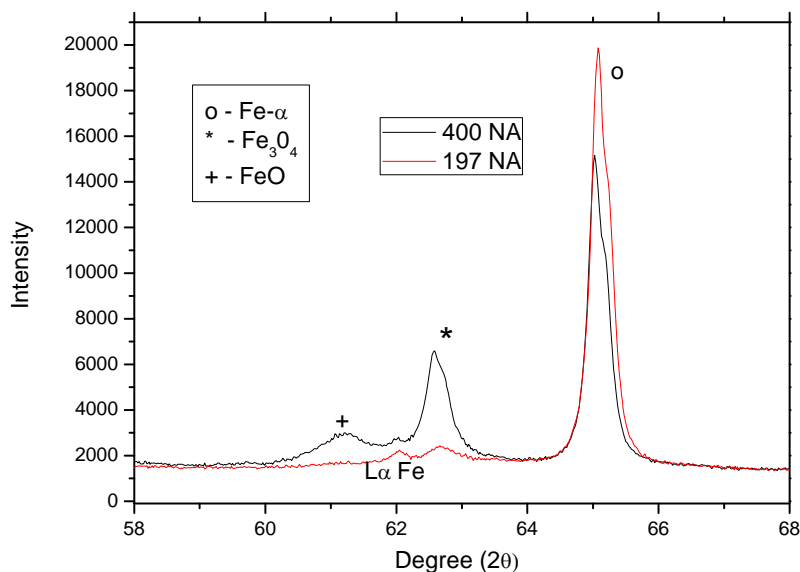
Figure 4:   Peaks of the XRD chosen for the semi-quantitative calculation.

Table 4:   Semi-quantitative analysis for the species contained in the XRD patterns.

	Non-activated NANOFER STAR 400	Activated NANOFER STAR 400	Non-activated NANOFER STAR 197	Activated NANOFER STAR 197	Activated NANOFER 25P
Fe	57%	57%	79%	79%	86%
Wuestite	17%	17%	~1-3%	~1-3%	~1-3%
Magnetite	25%	26%	17%	17%	10%

The detail characterisation of the nZVIs milled with alumina is summarized in Table 5.

Table 5:   Overview of the physical and chemical properties and reactivity parameters of NANOFER nZVIs

	NANOFER 25P	NANOFER 25S	NANOFER STAR
Short description	nZVI without stabilization (pyrophoric)	nZVI stabilized with organic layer	nZVI stabilized with oxidic layer
Chemical composition	Fe (70-85), O (5.5-14.5), Si (1.3-1.7), Al (0.06-0.08), others like Cu, Cr, Mn, Tb, Zn, P, Ni, Ti, S (0.4-0.7)	Fe (70-85), O (5.5-14.5), Si (1.3-1.7), Al (0.06-0.08), others like Cu, Cr, Mn, Tb, Zn, P, Ni, Ti, S (0.4-0.7)	Fe (70-85), O (5.5-14.5), Si (1.3-1.7), Al (0.06-0.08), others like Cu, Cr, Mn, Tb, Zn, P, Ni, Ti, S (0.4-0.7)
Average primary particle size ± RDS [nm] (specify: method applied)	71.8±1.5 (same as for Nanofer STAR) Scanning electron microscopy	71.8±1.5 (same as for Nanofer STAR) Scanning electron microscopy	71.8±1.5 (for batch 197) Scanning electron microscopy
Specific surface area [m^2/g]	15-24 (same as for Nanofer STAR)	15-24 (same as for Nanofer STAR)	15-24
Density [kg/m^3] (specify: true density, bulk density as powder, effective particle density with water-filled pores)	1120-1180 (same as for Nanofer STAR) Bulk density as a powder	1120-1180 (theoretical value, material available only in suspension) Bulk density as a powder	1120-1180 Bulk density as a powder
Sedimentation rate [nm/min]	N/A	N/A	N/A

	NANOFER 25P	NANOFER 25S	NANOFER STAR
Zeta potential [mV] (specify: suspension fluid and pH)	2.3 8.7	-41.5; pH 8.7 for 0.1 % suspension	4.6; pH 8.7 for 0.1 % suspension
Type of stabilizers (in suspension)	N/A	PAA – polyacrilic acid	N/A
Content of stabilizers [%]	N/A	3	N/A
Zeta potential in presence of stabilizer [mV] (specify: suspension fluid and pH)	N/A	N/A	N/A
Reactivity data towards target toluene	N/A	N/A	N/A
Expected products after aging	Fe_xO_y, FeOOH, $Fe(OH)_x$ (dependent on environment)	Fe_xO_y, FeOOH, $Fe(OH)_x$ (dependent on environment)	Fe_xO_y, FeOOH, $Fe(OH)_x$ (dependent on environment)

To assess the reactivity toward oxidation, nZVI nanoparticles were diluted in milliQ (18.2 MΩ-cm) water at different aging times (0 up to 7 days) inside a nitrogen-filled glove box without stirring until the analysis. Direct sunlight exposure was avoided. Prior to use, water was flushed with nitrogen for a minimum of 4 hrs to purge the oxygen. Then, nZVI particles were added to obtain a solution of 5 g/L.

The pH was the first parameter to be analysed (Figure 5), due to the fact that changes in the pH provide information about the aqueous oxidation of NP. As nZVI oxidizes to ferrous and/or ferric iron, the pH increases, hydrogen evolves, and oxidisable species are consumed (H+). During the seven days of the experiment, the pH values remained constant for NANOFER 25S nanoparticles, while in the case of NANOER STAR, the pH increased up to 10 (Figure 5). The largest pH changes for NANOFER STAR occurred during the first three days. This indicated that oxidation of NANOFER STAR took place over three days, while NANOFER 25S was more stable. Knowing that NANOFER STAR is designed to be more stable against oxidation, these pH data indicate that NANOFER 25S was already oxidized, while NANOFER STAR was more metallic and sensitive to oxidation.
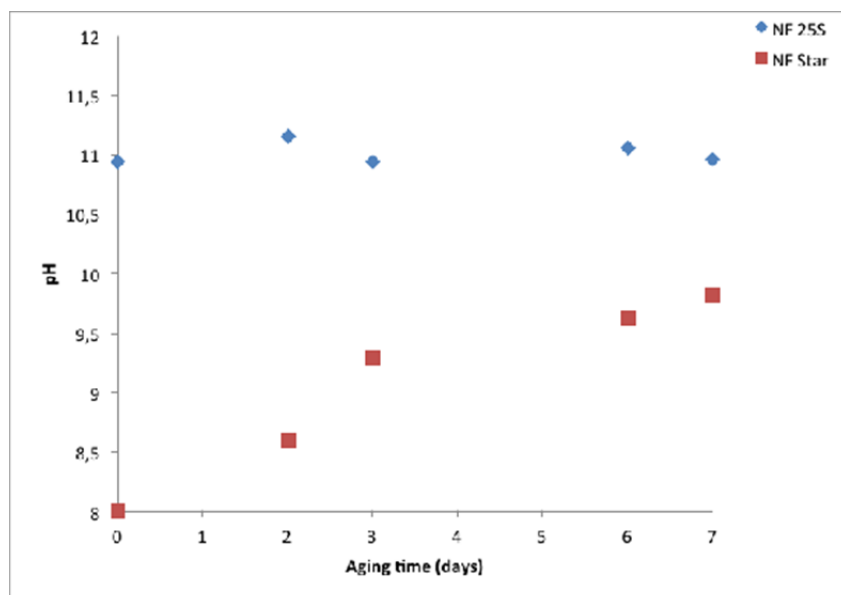
Figure 5: pH evolution during the first week of aging of the nZVI samples

TEM images obtained from fresh nZVI nanoparticles show that the core-shell structure was more pronounced in the case of NANOFER STAR. Energy-dispersive X-ray spectroscopy (EDX) profile measurements of freshly prepared samples (Figure 6) confirmed that the oxygen content was higher at the edges of both nZVI.
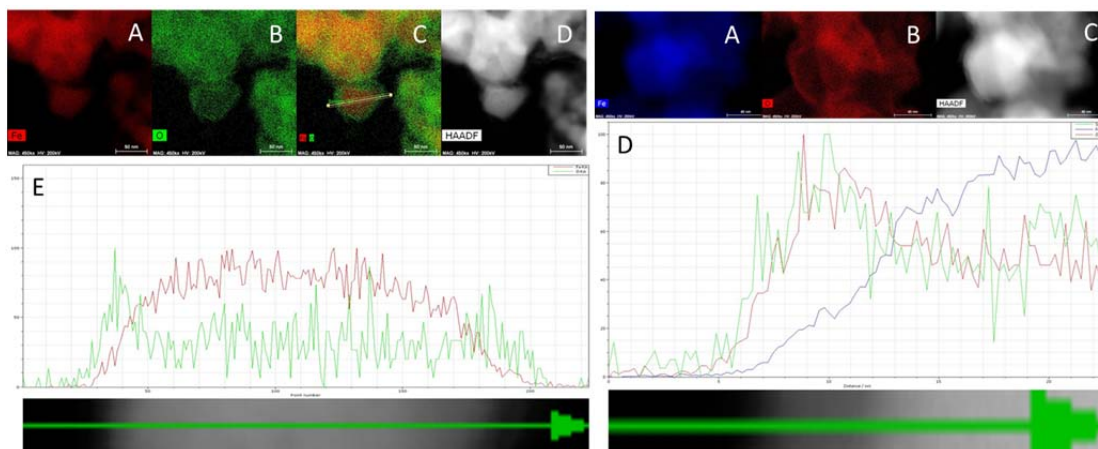
Figure 6: HAADF-STEM, EDX maps and profiles of freshly prepared NANOFER 25S (left) and NANOFER STAR (right). A) Fe map, B) O map, C) overview map and D) HAAD, E) EDX profile (determined following the green trajectory line indicated in the HAADF-STEM image).

After 2 days of aging, the TEM images suggest that the oxide layer became irregular in shape, and probably led to the formation of smaller nanoparticles. EDX profile measurements for NANOFER 25S con-firmed the presence of oxygen all along the trajectory line after two days. This means that even the core of the particles was oxidized. In the case of NANOFER STAR, the amount of oxygen along the trajectory line remained slightly greater at the edges after two days. However, after seven days the oxide surface layer also disappeared in NANOFER STAR with the EDX profiles indicating that the oxygen is homogeneously distributed.

Based on magnetic measurements, XAS at the Fe K-edge and XRD, we estimated the amount of Fe(0) and iron oxides in the freshly prepared nZVI. At t=0, the NANOFER STAR sample exhibited a greater percentage of Fe(0) (43%) than NANOFER 25S (29%) (Table 6). Fe(0) content decreased over time, while the iron oxide content increased for four days. Percentages of Fe(0) and iron oxides (not only magnetite) were shown (Table 6). For both NANOFER 25S and NANOFER STAR, magnetite was the main oxidation product found.

Table 6:   Weight percentage of Fe(0) and iron oxides for NANOFER 25S and NANOFER STAR over four days based on magnetic measurements.

Aging Time (Days)	NANOFER25S			NANOFERStar		
	Wt % metal	Wt % Total Iron Oxides	Wt % Other Oxides except magnetite	Wt % metal	Wt % Total Iron Oxides	Wt % Other oxides except magnetite
0	29%	71%	21%	43%	57%	4%
2	13%	87%	20%	29%	71%	24%
4	4%	96%	24%	31%	69%	18%

5.1.2   Reactivity of NANOFER NPs

Reactivity with the main target contaminants

At the beginning of the research the experiments focused on a comparison of the reactivity of the commercially available iron NANOFER 25S, which is produced as a modified aqueous suspension, with a new air-stable product NANOFER STAR. Besides the NANOFER STAR particles were modified with different stabilizers (Figure 7). The main target contaminants were chlorinated hydrocarbons (CHCs) as Perchlorethylene (PCE), Trichlorethylene (TCE), dichlorethens (cis-DCE).
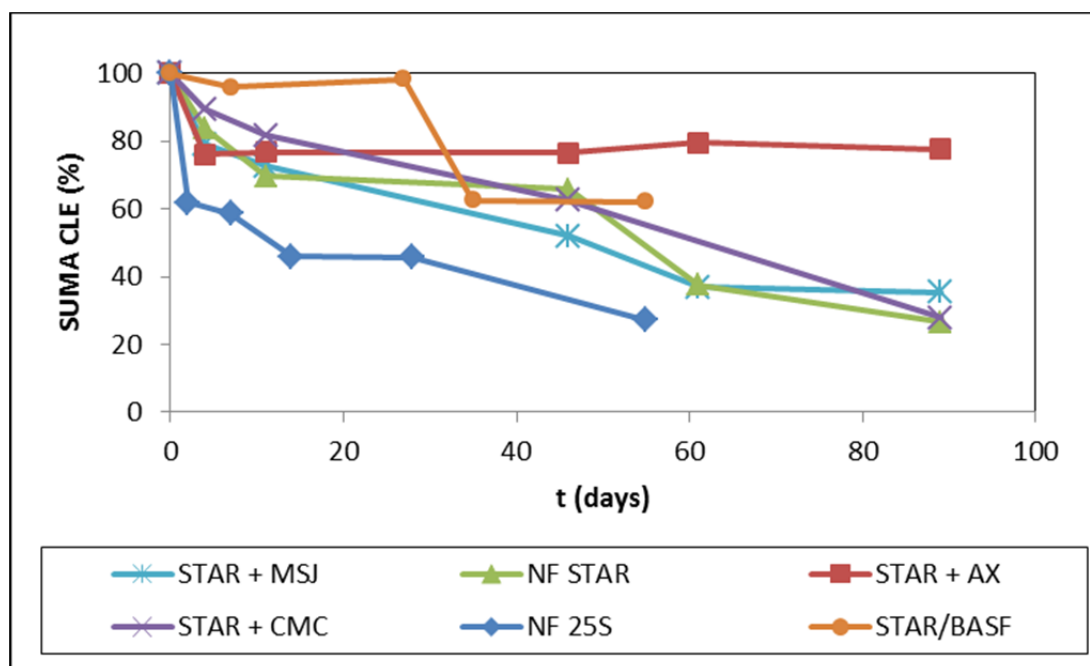
Figure 7:   Comparison of concentrations of chlorinated ethenes treated by NANOFER 25S and non-activated NANOFER STAR with different surface modifications

The results show that the additional surface modification of non-activated NANOFER STAR gives ambiguous results. The PAA (Polyacrylid acid) modified iron resulted in poor degradation of the chlorinated ethenes. The best modification seems to be NANOFER STAR + MSJ, which later also showed good migration properties. However, in com-parison with NANOFER 25S, as a commercial product, the reactive (and later migration) Capabilities were still lower. Nevertheless, NANOFER STAR + MSJ can be beneficial for certain real applications in the field because of the longer period of time during which it can be active in the subsurface. In general, it can be stated that the non-activated powder – NANOFER STAR has a slower reactivity than NANOFER 25S due to gradual disintegration of the surface oxide layer and that migration of the NANOFER STAR powder is slower because of the absence of smaller fractions with high mobility.

In the next series of tests, special attention was paid to the activation process of NANOFER STAR. Due to the fact that we determined that the particles need to be activated prior their application to increase their reactivity with contaminants, additional surface modification with different stabilizers (PAA and CMC) after the activation process was tested and compared (Figure 8, Figure 9).
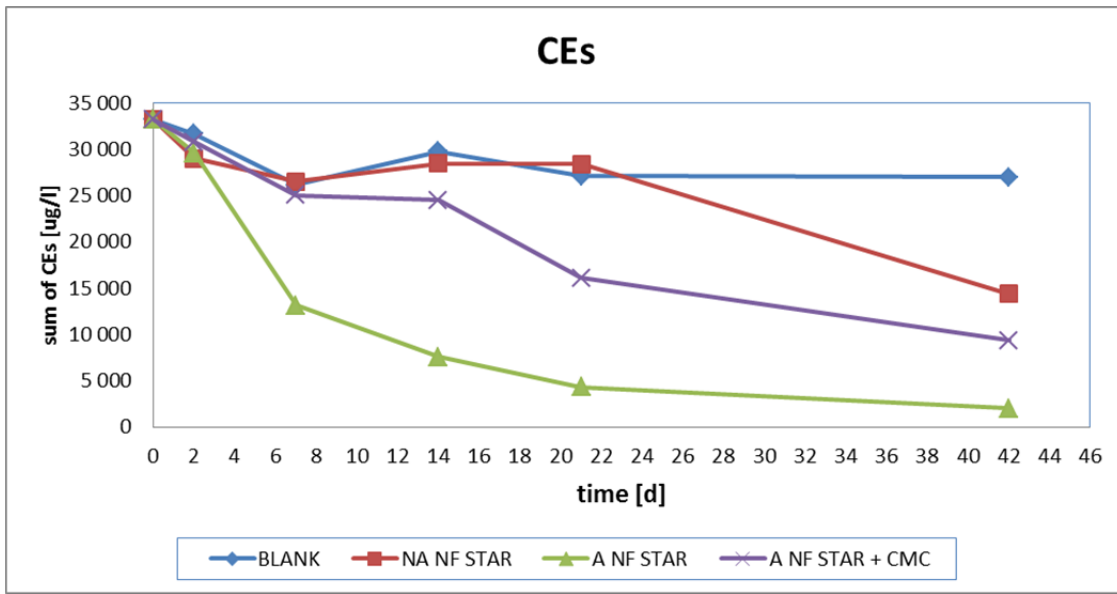
Figure 8: Comparison of the rate of CE degradation (PCE, TCE, cis-DCE) by freshly prepared NANOFER STAR (NA), activated NANOFER STAR (A) and activated NANOFER STAR additionally modified by CMC.
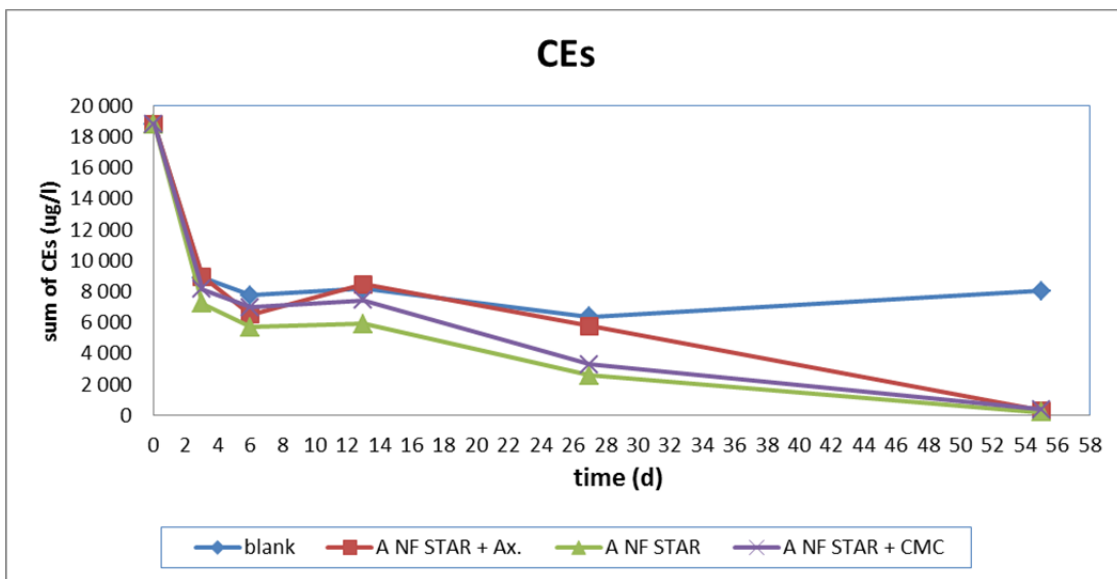
Figure 9: Comparison of the rate of CE degradation (PCE, TCE, cis-DCE) by activated NANOFER STAR additionally modified by different stabilizers.

The additional surface modification of A NANOFER STAR was tested to improve the reactivity and migration properties of the particles. In the both cases of modification, a slight prolongation of the reaction time was observed but after almost two months the same rate of CE degradation was achieved.

General application area

In addition to CHC reactivity, NANOFER particles were tested on the chromium (Cr(VI)) contamination. The concentration trends of Cr(VI) as a function of the nZVI concentration for the studied nanoparticles are shown in Figure 10. As it can be seen, the Cr(VI) removal was linearly proportional to the amount of nZVI applied. The slope varied with the type of nZVI and depended on the activation process. The most reactive NANOFER 25P nanoparticles revealed very little differences between the activated and the non-activated state. On the contrary, the surface stabilized nanoparticles in the non-activated state, UA STAR 197 and 400, showed very low reactivity compared to NANOFER 25P. However, once activated, these nanoparticles displayed a significant improvement in reactivity. In the case of A STAR 197, the removal capacity of Cr(VI) increased nearly five times more than in the case of UA STAR 197, reaching values slightly above half the reactivity of the 25P nanoparticles. For A STAR 400, the increase was also considerable since the reactivity improvement was more than three times higher than in the case of UA STAR 400. The observed differences in reactivity can be explained mainly by the characteristics of the oxide layer (showed in Figure 1).
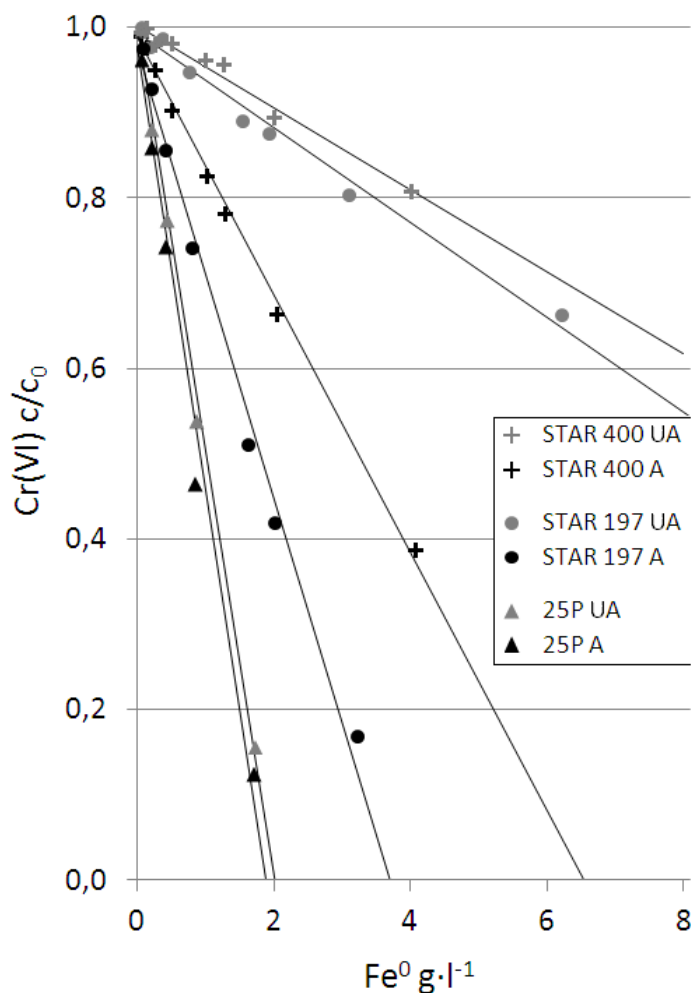

Figure 10: Chromium depletion of different types of NANOFER irons in an activated and non-activated state at different ZVI concentrations.

5.2   Milled nZVI particles (FerMEG12)

Responsible partner: UVR-FIA GmbH

5.2.1   Physical-chemical properties of FerMEG12

For the analysis of the particle size, shape, surface and structure, a Phenom electron microscope was used as a supplementary investigatory tool. The basic raw material ATOMET 57, a coarse, high purity granulated iron powder from Rio Tinto, Quebec Metal Powders Ltd. consists of flakes as well as spherical and irregular particles (Figure 11, left). The pre-milling product contains small, compact particles. The surface of some of the particles is enlarged by small particles, which seem to be forgotten (Figure 11, centre). The shape of the nano-structured (less than 100 nm) final product is platelet-like only (Figure 11, right).
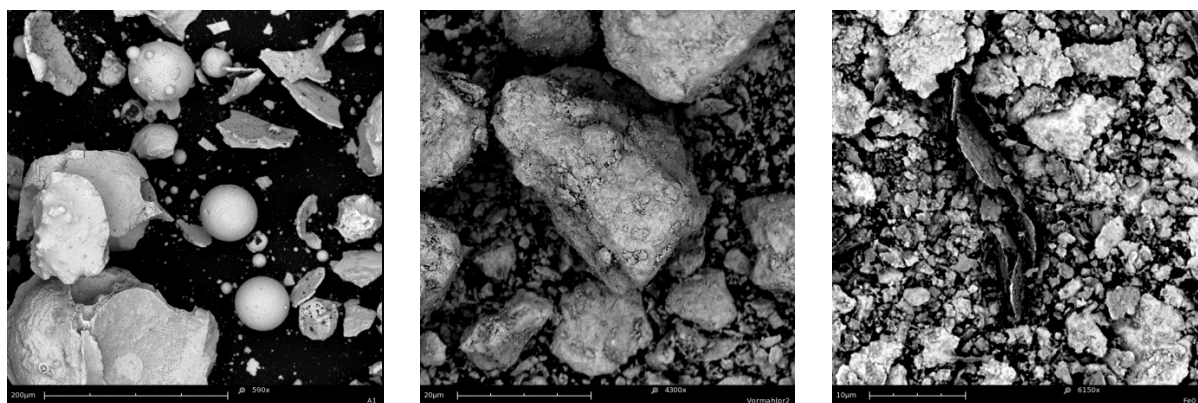
Figure 11: SEM picture of milled particles: left - starting product ATOMET57, centre - pre-milling product, right – FerMEG final nZVI

The measurement of nZVI content in a slurry or as a powder is based on the measurement of the volume of hydrogen released during the chemical reaction of zero-valent iron and sulphuric acid. The volume of hydrogen is directly proportional to the amount of zero-valent iron; the amount of iron-oxides does not influence the volume of generated hydrogen but merely slows down the reaction speed. The weight content of iron particles in monoethylen glycol (MEG) is approximately 25 – 30 %.

According to the Brunauer–Emmett–Teller theory (the BET method) the specific surface area ranges from 12 to 18 m²/g.

A detailed characterisation of the milled nZVIs is summarized in Table 7.

Table 7:   Overview of the physical and chemical properties and the reactivity parameters of Fer-MEG12

	FerMEG12
Short description	nZVI flakes in monoethylene glycol (MEG) suspension
Mode of action	-
Chemical composition	Fe
Average primary particle size ± RDS [nm] (specify: method applied)	Sauter mean diameter ~ 50 nm
Specific surface area [m^2/g]	18 m²/g
Density [kg/m^3] (specify: true density, bulk density as powder, effective particle density with water-filled pores)	not applicable
Sedimentation rate [nm/min]	-
Zeta potential [mV] (specify: suspension fluid and pH)	-
Type of stabilizers (in suspension)	none
Content of stabilizers [%]	-
Zeta potential in presence of stabilizer [mV] (specify: suspension fluid and pH)	-
Expected side-reactions	-
Expected products after aging	Fe oxides/ hydroxides
Other specifities	-

5.2.2   Reactivity of FerMEG12

Reactivity with the main target contaminants

The reactivity of the milled irons was tested on real contaminated water from the field (Solvay site, Switzerland). The kinetics of the CHC degradation and a comparison of the reactivity properties of different FerMEG12 batches are shown in Figure 12 and Figure 13, respectively.
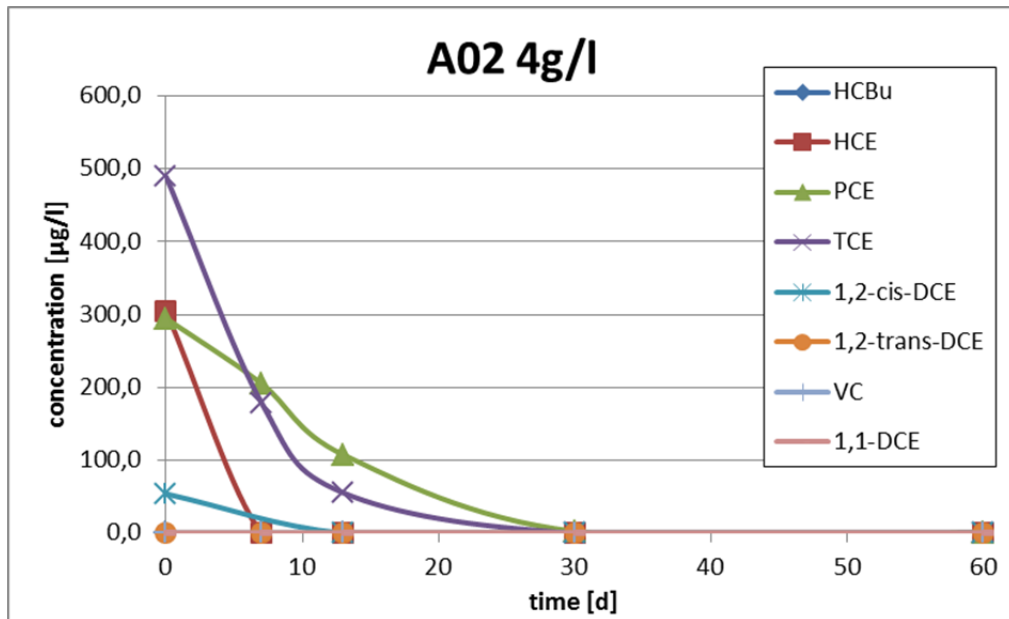
Figure 12: Rate of degradation of different pollutants using milled iron A02
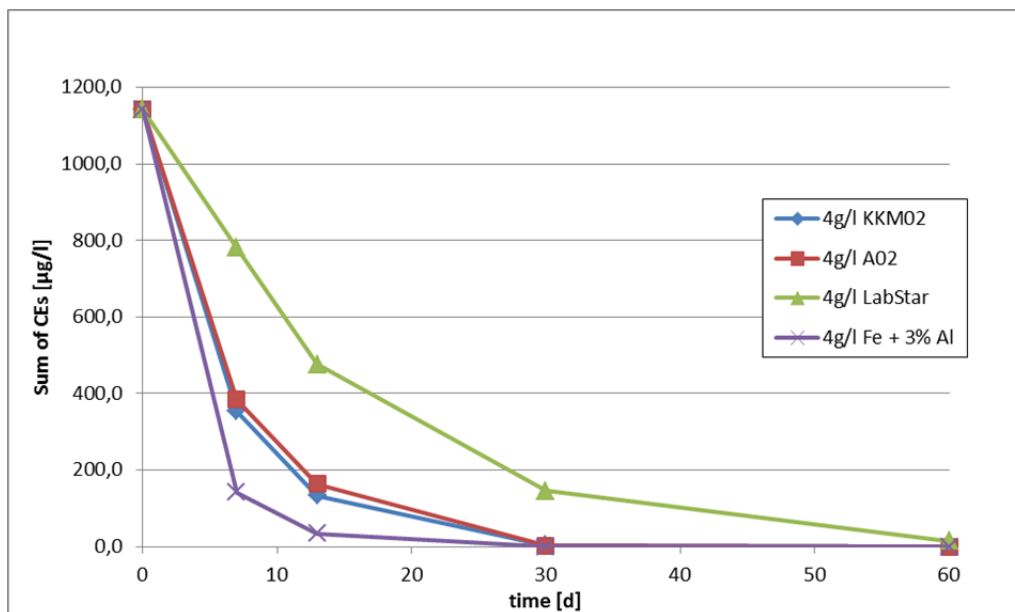
Figure 13: Comparison of the rate of CE degradation by the different types of milled iron FerMEG12

5.3   Milled ZVI nanoparticles with alumina as an abrasive

Responsible partner: .CTM

After a long period spent fine tuning the milling process, two different samples were selected for further characterization.

- NA 64, using a Ø 5mm ball composed of low carbon steel (AISI 1010) and an alumina concentration of 53.6 g·l-1, and

- NA 84, using a Ø 0.5mm ball composed of high carbon steel (0.80-1.20%) and an alumina concentration of 80.4 g·l-1.

5.3.1   Physical and -chemical properties of the milled irons milled with alumina

Size characterization (Figure 14) is a key feature since mobility and reactivity have a strong dependency to these parameters.
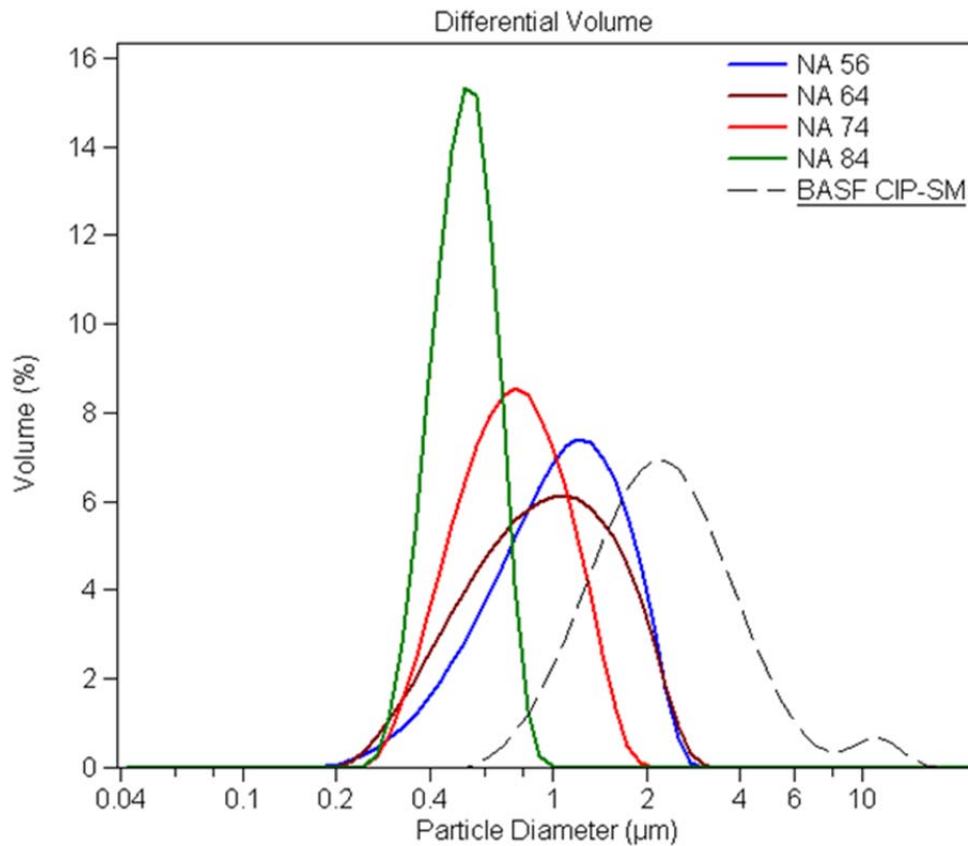
Figure 14: Granulometric distribution obtained by laser diffraction of: NA 56, NA 64, NA 74, NA 84 and the initial powder.

The SEM images of the most promising batch NA 84 are shown in Figure 15. A detailed characterisation of the milled nZVIs with alumina is summarized in Table 9. The addition of micronized alumina was intended to behave as a micro grinding media, where abrasive particles would act as a small irregularities coating the grinding balls, being a pressure spots between the grinding balls and the flakes. Previous results showed that, after the addition of alumina, iron flakes from the initial iron powder disappeared meaning that the proposed mechanism was working.

However, further analysis stated that the main responsible for the nanoparticle production was the alumina abrasion onto the grinding steel balls. Table 8, shows the expected total iron concentration according to the initial iron powder supplied into the vials and the real recovered iron concentration. As can be seen, final total iron concentration was several times higher than the expected concentration in both tests (NA 64 and NA 84). These results demonstrate a large iron abrasion from the grinding media. Graphically, in Figure 15 micro alumina particles had iron residues adhered on the edges, possibility due to shear action which can explain the working mechanism.

Figure 15: SEM image of the sample NA 84.

Table 8:   Expected and real iron concentrations in MEG at the end of the milling (expressed in $g \cdot L^{-1}$), and the carbon content of the particles (in %).

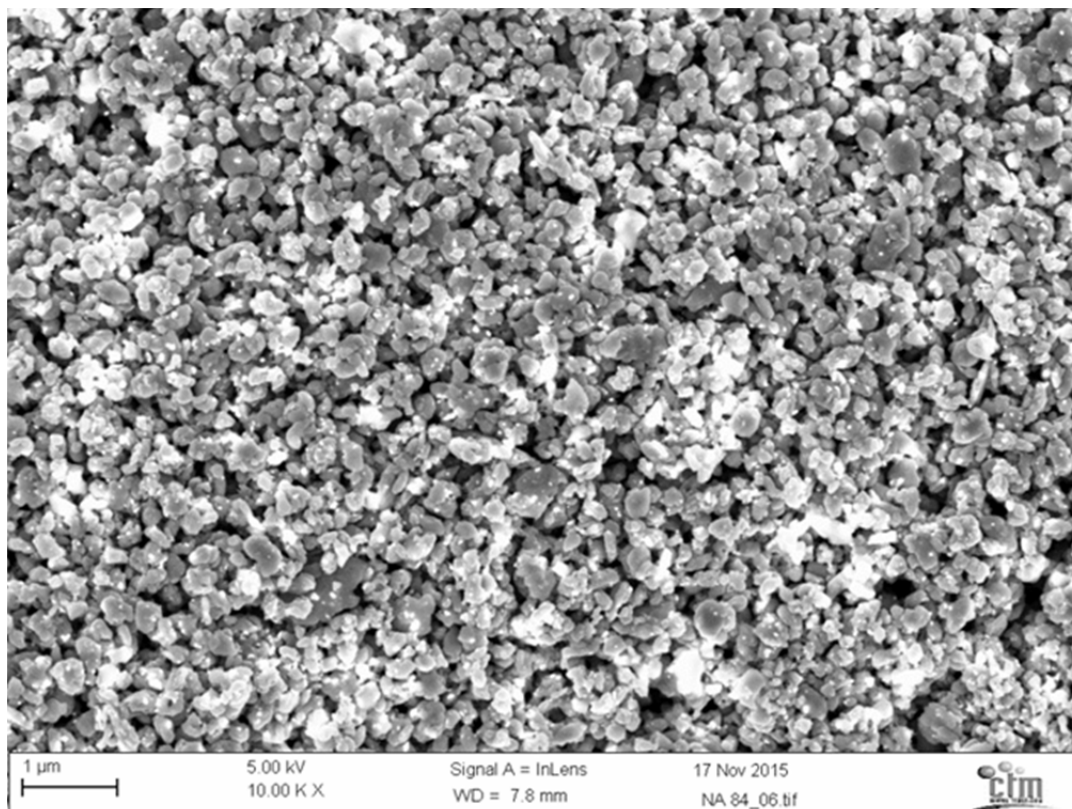|	NA 64	NA 84
Expected [Fe]	15.0	15.0
Real [Fe]	96.7	148.3
Expected C	≤0.1	≤0.1
Real C	2.10	2.69

Table 9:   Overview of the physical and chemical properties and reactivity parameters of iron milled with alumina

	Milled nZVI with an alumina
Short description	nZVI produced by ball milling and microscale alumina additive.
Mode of action	---
Chemical composition	Fe (0): 78% (NA 64); 74% (NA 84) C: 2.10% (NA 64); 2.69% (NA84)
Average primary particle size ± RDS [nm] (specify: method applied)	460 (NA64); 160 (NA84) SEM by number 470 (NA 64); 390 (NA84) LD by number 1001 (NA 64); 520 (NA84) LD by volume 760 (NA 64); 620 (NA 84) DCS by volume * Narrow distribution, low agglomeration.
Specific surface area [m^2/g]	20.0 (NA64); 29.6 (NA84)
Sedimentation rate [$mm \cdot h^{-1}$]	5.64 (NA 64); 1.39 (NA 84)
Zeta potential [mV] (specify: suspension fluid and pH)	+27mV at 9.6 pH in water. (yes, it is positive, regardless of the alumina and MEG))
Type of stabilizers (in suspension)	Mono Ethylene Glycol
Zeta potential in presence of stabilizer [mV] (specify: suspension fluid and pH)	(MEG and alumina at 1g.l^{-1}) +25mv at 10.0 pH in water.
Reactivity data towards target toluene	Not tested. Excellent (higher than 25P) against Cr(VI), TCE and PCE also once normalized by SSA and Fe(0) content.
Expected side-reactions	Dechlorinating products not detected (1,1-Dichloroethylene, cis-Dichloroethylene, trans-1,2-Dichloroethene and Vinyl Chloride)
Expected products after aging	Unknown
Other specifities	Very small 5-10nm crystal lattice. First mobility results are promising showing excellent mobility which is in agreement with the exceptional low sedimentation rates.

5.3.2   Reactivity of irons milled with alumina

The NPs milled with alumina were tested and their physical and chemical properties and reactivity were compared with commercially available NPs.

Figure 16: Depletion curves of CEs for the produced nanoparticles NA 64, NA 84 and the commercial reference irons 25P, STAR and A01.

Trichloroethylene (TCE) and Tetrachloroethylene (PCE) were selected as classic pollutants of the CHC family. Following the same experimental set, CTM developed particles were tested together with commercial ones, Figure 16. Both contaminants were tested simultaneously at concentrations simulating a real site. It can be concluded that the performance of all nanoparticles is much higher, the reactivity towards PCE is the clearest example of where nanoparticles can eliminate high concentrations of PCE with iron concentrations below $1g \cdot L^{-1}$.

Figure 17 shows a comparison of the Cr(VI) elimination with NPs at different concentrations. The NPs milled with alumina show a much better performance than the other NPs and it is a very promising result. This superior reactivity of milled NPs with alumina comes first from an absence of an oxide layer, but it is thought that the great amount of superficial irregularities that form a great number of reactive sites and the presence of a very fine nanostructure inside the milled particles also play a key role.
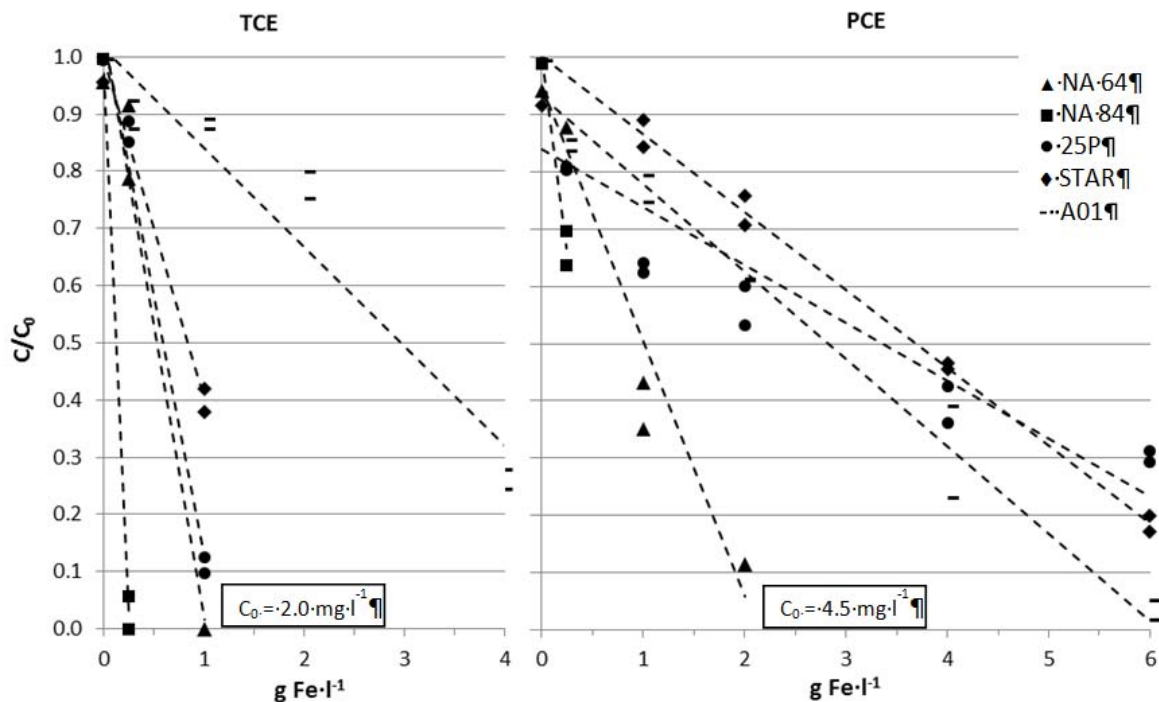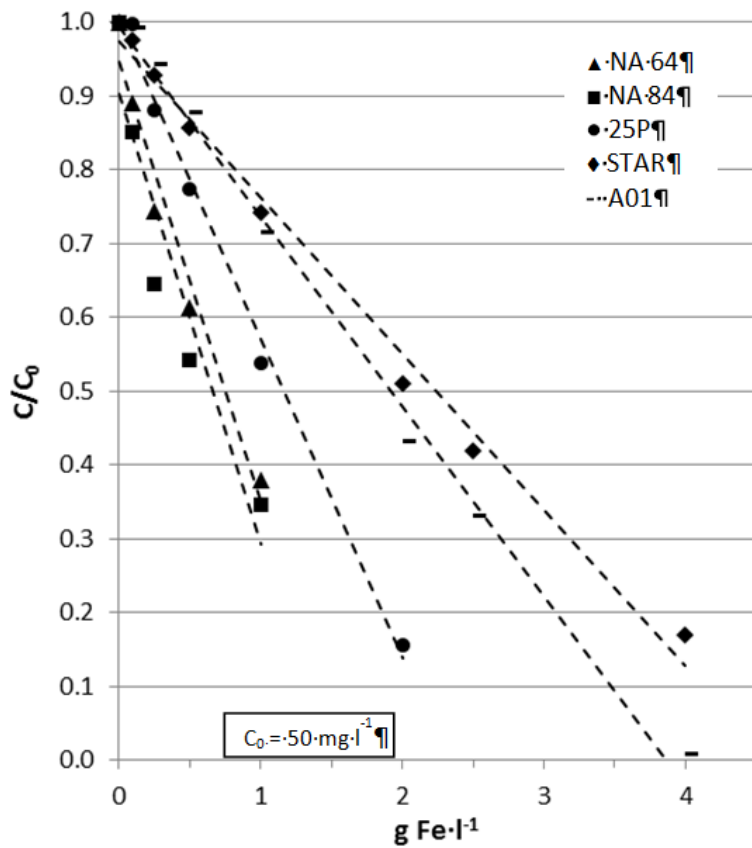
Figure 17: Depletion curves of Cr(VI) for the produced nanoparticles NA 64, NA 84 and the commercial reference irons 25P, STAR and A01.

In addition, the column tests were performed to check and compare the migration properties of the milled irons with commercial nZVIs also showed good results (Figure 18). The y-achse (Delta frequency) means the response of the detector.
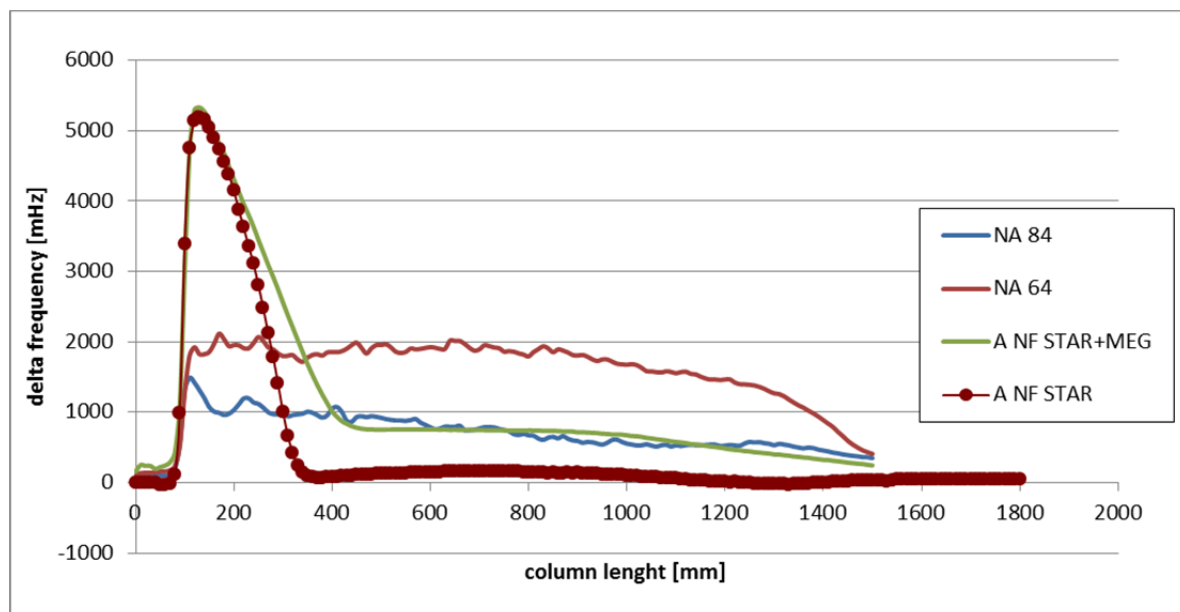
Figure 18: Comparison of the migration ability of different nZVIs in porous media

6　Summary and Overview of Particles Abilities and their Application area

Table 10:　Overview of identified application areas/potential of particles

Particle Type	Reaction types supported by the particles						Reaction mode				Recommendation for site conditions					Stabilizer needed		General rules for use				Possible spin-off applications			Development status		
	Oxidation	Reduction	Hydrophobic sorption	Sorption of metals/metalloids	Support of biology. treatment	Hydrolysis	Reactive component consumed	Additional reagents needed	Gaseous products formed		Anaerobic	Aerobic	pH << 7	pH ≈ 7	pH > 7	yes	no	Inertization of suspension needed	Disperser needed			wastewater			Tested at field scale	Ready for up-scaled testing	Research at laboratory scale
NANOFER (25P, 25S, STAR)		x		x	x		x		x		x			x	x		x		x			x			x	x	X
FerMEG12		x		x	x		x		x		x			x	x	x			x			x			x	x	X
Milled iron with alumina		x		x	x		x		x		x			x	x	x			x			x					x

Table 11: List of selected contaminants degradable (**+** successfully tested, **-** not applicable, **L** likely, but not tested), adsorbed or otherwise treatable (**t**)

Particle Type	Halogenated hydrocarbons										Non-halogenated hydrocarbons						Others				
	Chlorinated Olefins (e.g.C2Cl4, C2HCl3, C2H2Cl2)	Brominated Olefins (e.g. C2H3Br)	Halomethanes (e.g. CCl4, CHBr3, CHBr2Cl …)	Saturated polyhalogenated (e.g. C2H3Cl3)	Dichloroethane, Dichloromethane	Aromatics, Phenols (low substitution degree, e.g. dichlorobenzene)	Aromatics, Phenols (high halogenation degree, e.g. PCBs, Pentachlorophenol)	Herbicides and pesticides (e.g. DDT, Lindane)	Pharmaceuticals (e.g. Iopromid)		BTEX	PAHs	Fuel oxygenates (MTBE, ETBE)	Petroleum hydrocarbons			Metals/Metallois (e.g. Cr(VI), Cd(II), As(III), As (V)	Nitro compounds (e.g. TNT, nitrobenzene)	Perchlorate		Further contaminants tested [1]
NANOFER (25P, 25S, STAR)	+	+	+	-	+	-	+	+	-		-	-	-	-			+	+	L		
FerMEG12	+	+	+	-	-	-	-	L	-		-	-	-	-			+	L	L		
Milled iron with alumina	+	L	L	-	-	-	-	L	-		-	-	-	-			+	L	L		

Table 12: Reactivity data for typical target contaminants

NPs	NP concentration	Contaminant	Initial contaminant concentration	Type of background solution	pH of background solution	Contaminant degradation		Corrosion	Fe⁰ efficiency	Additional data
	[g L^{-1}]		[mg L^{-1}]			k_{obs} [h^{-1}]	k_{SA} [L m² h^{-1}]	k_{H2} [h^{-1}]	$\in$ [%]	
NANOFER 25S	1.1	PCE	50	F.l.s F.l.m F.l.h	7.6 7.8 8.2	2.6x10^{-3} 1.9x10^{-3} 1.7x10^{-3}	1.0x10^{-4} 0.76x10^{-4} 0.68x10^{-4}	5.3x10^{-4} 5.4x10^{-4} 4.8x10^{-4}	5.2	
NANOFER 25S	0.25	Cr	46.8	F.l.m	12	0.034	1.4x10^{-3}			A = 2.3×10^{-3} L g$_{NP}^{-1}$ min^{-1}
Optimized NANOFER Star	1	PCE	50	F.l.m	n.a.		1.79x10^{-5}			For activated NANOFER STAR: k_{SA} = 1.67x10^{-5} [L m² h^{-1}]
FerMEG12	1	TCE	11	Soft (F.l.s)	7.64	1.58x10^{-3}	8.80x10^{-5}		18	

7   List of References

DL 2.1; Černík M., Slunský J., Thümmler S. (2015) NanoRem Deliverable DL 2.1 Design, Improvement and Optimized Production of Nanoparticles -Zero-Valent Iron Nanoparticles – nZVI. NanoRem FP 7 Project GA No 309517. www.nanorem.eu

Filip, Jan, František Karlický, Zdeněk Marušák, Petr Lazar, Miroslav Černík, Michal Otyepka, and Radek Zbořil. "Anaerobic Reaction of Nanoscale Zerovalent Iron with Water: Mechanism and Kinetics." The Journal of Physical Chemistry C 118, no. 25 (June 26, 2014): 13817–25. doi:10.1021/jp501846f.

Klimkova, Stepanka, Miroslav Cernik, Lenka Lacinova, Jan Filip, Dalibor Jancik, and Radek Zboril. "Zero-Valent Iron Nanoparticles in Treatment of Acid Mine Water from in Situ Uranium Leaching." Chemosphere 82, no. 8 (February 2011): 1178–84. doi:10.1016/j.chemosphere.2010.11.075.

Liu, Y., Choi, H., Dionysiou, D., & Lowry, G. V. (2005a). Trichloroethene hydrodechlorination in water by highly disordered monometallic nanoiron. Chemistry of Materials, 17(21), 5315-5322.

Liu, Yueqiang, and Gregory V. Lowry. "Effect of Particle Age (Fe 0 Content) and Solution pH On NZVI Reactivity: H 2 Evolution and TCE Dechlorination." Environmental Science & Technology 40, no. 19 (October 2006): 6085–90. doi:10.1021/es060685o.

Li, Xiao-qin, Daniel W. Elliott, and Wei-xian Zhang. "Zero-Valent Iron Nanoparticles for Abatement of Environmental Pollutants: Materials and Engineering Aspects." Critical Reviews in Solid State and Materials Sciences 31, no. 4 (December 2006): 111–22. doi:10.1080/10408430601057611.

Lowry, Gregory V., Kelvin B. Gregory, Simon C. Apte, and Jamie R. Lead. "Transformations of Nano-materials in the Environment." Environmental Science & Technology 46, no. 13 (July 3, 2012): 6893–99. doi:10.1021/es300839e.

Sun, Yuan-Pang, Xiao-qin Li, Jiasheng Cao, Wei-xian Zhang, and H. Paul Wang. "Characterization of Zero-Valent Iron Nanoparticles." Advances in Colloid and Interface Science 120, no. 1–3 (June 2006): 47–56. doi:10.1016/j.cis.2006.03.001.

Ramakrishna, D. M., & Viraraghavan, T. (2005). Environmental impact of chemical deicers–a review. Water, Air, and Soil Pollution, 166(1-4), 49-63.

Wei, Y. T., Wu, S. C., Yang, S. W., Che, C. H., Lien, H. L., & Huang, D. H. (2012). Biodegradable surfactant stabilized nanoscale zero-valent iron for in situ treatment of vinyl chloride and 1, 2-dichloroethane. Journal of hazardous materials, 211, 373-380.